Strained Lattice with Persistent Atomic Order in Pt_3Fe_2 Intermetallic Core–Shell Nanocatalysts

Sagar Prabhudev,[†] Matthieu Bugnet,[†] Christina Bock,[‡] and Gianluigi A. Botton[†,*]

[†]Department of Materials Science and Engineering, McMaster University, Hamilton, Ontario, Canada L8S 4L8 and [‡]National Research Council, Ottawa, Ontario, Canada K1A 0R6

ABSTRACT Fine-tuning nanocatalysts to enhance their catalytic activity and durability is crucial to commercialize proton exchange membrane fuel cells. The structural ordering and time evolution of ordered Pt_3Fe_2 intermetallic core–shell nanocatalysts for the oxygen reduction reaction that exhibit increased mass activity (228%) and an enhanced catalytic activity (155%) compared to Pt/C has been quantified using aberration-corrected scanning transmission electron microscopy. These catalysts were found to exhibit a static core–dynamic shell regime wherein, despite treating over 10 000 cycles, there is negligible decrease (9%) in catalytic activity and the ordered Pt_3Fe_2 core remained virtually intact while the Pt shell suffered a continuous enrichment. The existence of this regime was further confirmed by X-ray diffraction and the compositional analyses using energy-dispersive spectroscopy. With atomic-scale two-dimensional (2-D) surface relaxation mapping, we demonstrate that the Pt atoms on the surface are slightly relaxed with respect to bulk. The cycled nanocatalysts were found to exhibit a greater surface relaxation compared to noncycled catalysts. With 2-D lattice strain mapping, we show that the particle was about −3% strained with respect to pure Pt. While the observed enhancement in their activity is ascribed to such a strained lattice, our findings on the degradation kinetics establish that their extended catalytic durability is attributable to a sustained atomic order.

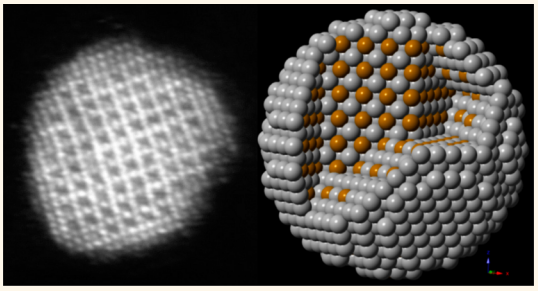

KEYWORDS: ordered nanocatalysts · proton exchange membrane fuel cells · Pt–Fe · lattice strain · scanning transmission electron microscopy

Research in designing electrocatalysts for various chemical reactions has witnessed a tremendous progress especially over the past decade, in terms of increasing their surface to volume ratios to reduce catalyst loading and, hence, mitigate the cost.[1,2] Currently, there is a great interest in devising such nanocatalysts to accelerate the oxygen reduction reaction (ORR) occurring at the cathode in a proton exchange membrane fuel cell (PEMFC).[3] Although carbon-supported platinum nanoparticles (Pt/C) were long thought of as an ideal ORR catalyst, it is now widely accepted to be an unrealistic choice owing to their exceedingly high costs.[3,4] Hence, various new catalyst designs are in vogue, with the intention to achieve higher activities and better durability compared to Pt/C, primarily dictated by a ground rule to induce compressive strain in the lattice by introducing 3*d* transition metals (M = Ni, Co, Fe, Cu, Cr).[5−10] Thus far, two prominent regimes are identifiable: the alloyed Pt–M systems mainly leading to bimetallic[11] and ternary[12] nanocatalysts and, a core–shell[13] design comprising a metal core and an enriched Pt shell. The Pt–Fe system, in particular, has gathered much attention in recent years not only as a better catalyst to Pt/C in PEMFCs but also because of its magnetic properties that are deployable in ultrahigh density information storage.[14] Disordered Pt–Fe core–shell nanoparticles reported hitherto lack a subsurface compressive strain in the Pt shell because there exists a poor *d*-overlap among Pt atoms, leading to decreased catalytic activity compared to that of bimetallic regimes.[15−17] Catalyst design among the bimetallic Pt–Fe ordered system in the recent past has been extremely limited mainly because of the conventional synthesis routes followed that lead to increased particle sizes due to

* Address correspondence to gbotton@mcmaster.ca.

Received for review April 17, 2013 and accepted June 17, 2013.

Published online June 17, 2013
10.1021/nn4019009

aggregation upon annealing[18−20] and partly because of the model-based calculations on the Pt−Fe system predicting a monotonically decreasing Pt profile in the subsurface layers as opposed to Pt−Co and Pt−Ni that were reported to be oscillatory.[15,21,22] Here we demonstrate a new intermetallic core−shell (IMCS) regime among Pt−Fe systems, comprising an ordered Pt_3Fe_2 core encapsulated within a bilayer Pt-rich shell. These catalysts exhibit the highest activity and extended durability compared to all other Pt−Fe designs reported in the literature.[18,23,24] While a comparative discussion on catalyst synthesis, electrochemical measurements, and XRD analysis of these catalysts with other Pt−Fe designs is presented in a recent article[19] by two of the authors, our current work investigates structural ordering as a design criterion for developing nanocatalysts with enhanced activity and extended catalytic durability. We show that the degradation kinetics in these IMCSs exhibit a static core−dynamic shell profile which could more generally be extended to explain enhanced durability observed in Pt−Co ordered systems reported recently,[16] over conventional disordered core−shell Pt−Co nanocatalysts.

RESULTS AND DISCUSSION

Pt_3Fe_2 IMCS nanocatalysts were synthesized by impregnating[19] Pt/C precursors with 0.1381 g of $Fe(NO_3)_3 \cdot 9H_2O$. Subsequent annealing in an 8% H_2/Ar atmosphere at 800 °C resulted in chemically ordered nanocatalysts with surface-segregated Pt-rich shells, as shown in Figure 1, typically with an average diameter of 3.2 nm. XRD analysis on the annealed samples revealed a slight increase in the crystallite size postannealing, which is known to be due to possible particle sintering.[18,25] We also found that the amount of Fe salt added primarily dictates the stoichiometry of ordered cores being formed. For example, although impregnating 0.0691 g of Fe salt resulted in a Pt_3Fe ordered core, the Pt was found to exhibit poorer surface segregation, in turn leading to a significant decrease in catalyst performance.[19,22,24]

Atomic-resolution STEM-HAADF images in Figure 1b,c clearly show the ordered Pt_3Fe_2 core architecture with

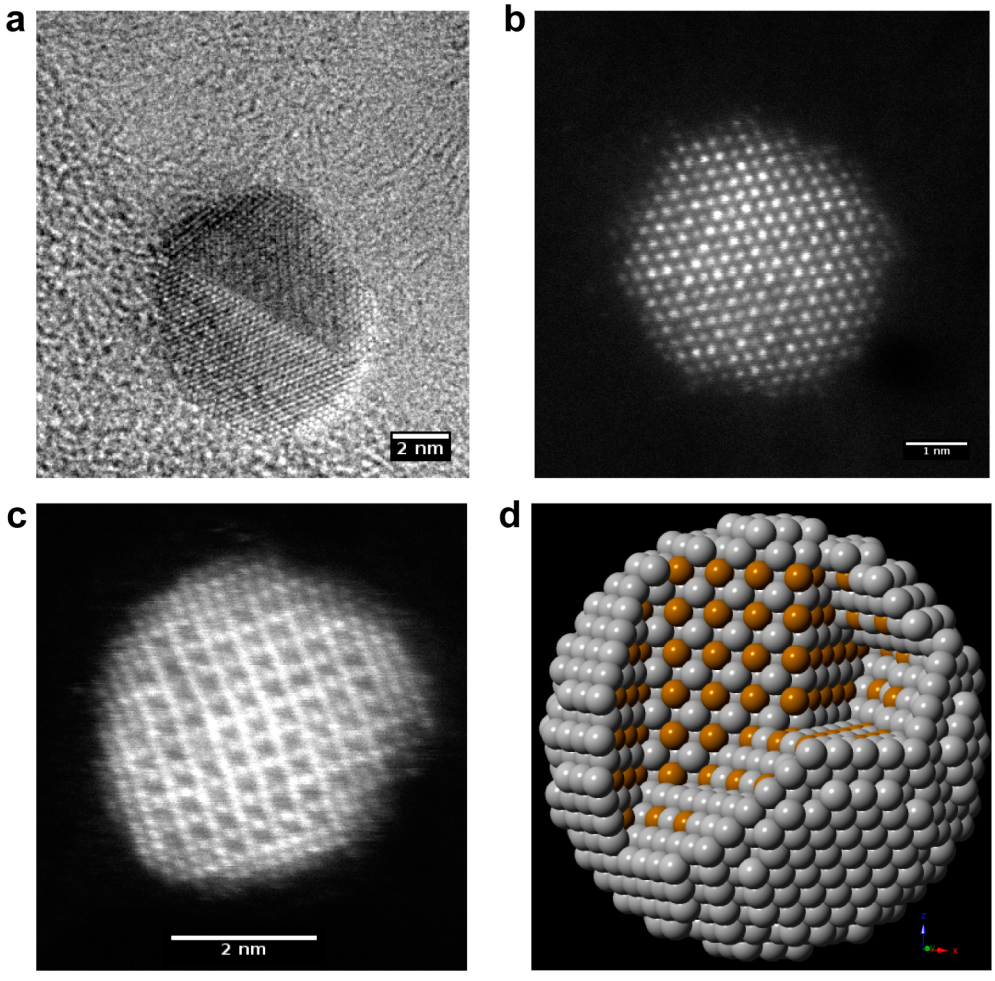

Figure 1. Atomic-resolution BF and HAADF images. (a) TEM bright-field (BF) image of an as-prepared Pt_3Fe_2 intermetallic core−shell nanocatalyst (IMCS). (b,c) STEM-HAADF images of Pt_3Fe_2 IMCS nanocatalysts showing alternating bright and dark intensities for Pt and Fe atomic columns, respectively, at the core. However, the shell is Pt-rich, as demonstrated by much brighter intensity at the surface that is further supported by multislice method image simulations (Supporting Information). (d) Three-dimensional model of a typical IMCS nanocatalyst. Pt and Fe atoms are represented by gray and yellow, respectively.

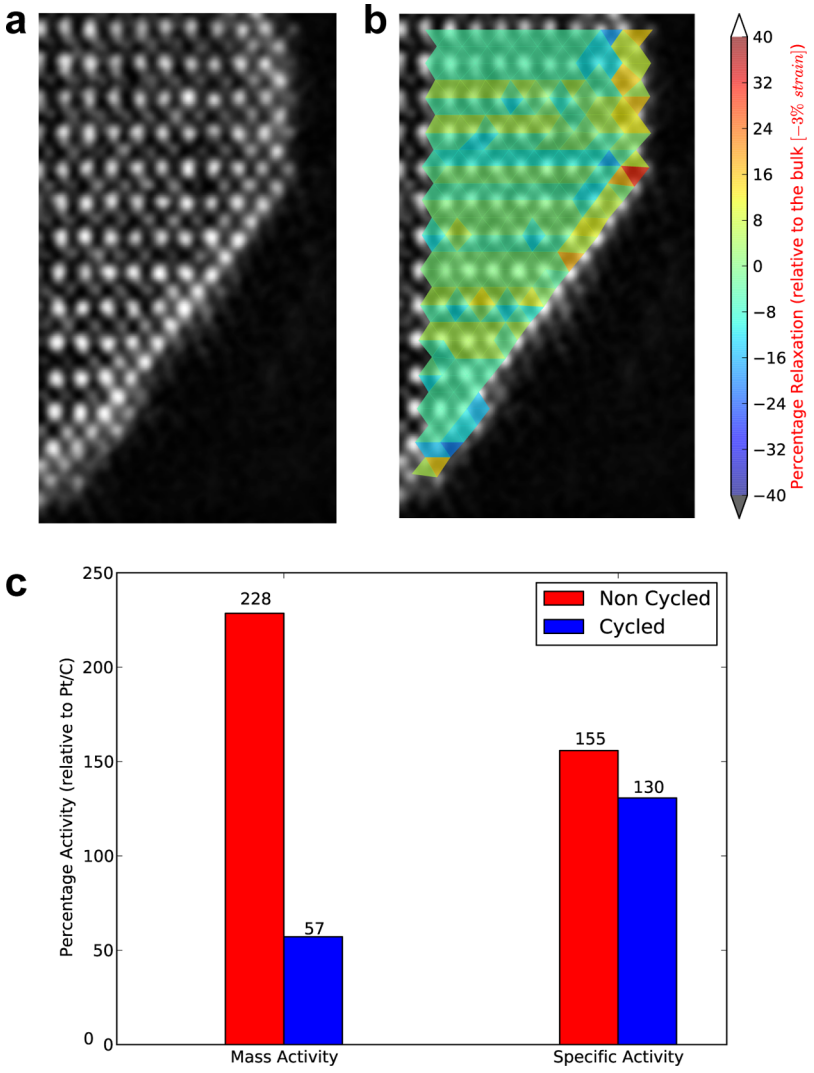

Figure 2. Structure, strain, and activity. (a) Magnified region of an IMCS catalyst nanoparticle acquired as a Gaussian filtered STEM-HAADF image demonstrating the ordered Pt_3Fe_2 core and Pt-rich shell at atomic resolution. (b) Two-dimensional lattice strain mapping (method described in the Supporting Information) of particle in (a) indicating a bulk strain of −3% at the core. The surface appears to be relaxed compared to the ordered core. (c) Bar plot indicating the enhancement in mass activity and the catalytic activity among Pt_3Fe_2 IMCS compared to Pt/C measured at similar testing conditions.

alternating bright and dark contrast, indicating the positions of Pt and Fe atomic columns, respectively (detailed interpretation of STEM-HAADF contrast aided with multislice method image simulations is discussed in the Supporting Information section 1, Figures S1 and S2). From these observations, it appears that the heat treatment induced a selective segregation of Pt at the surface of the nanoparticle, typically two atomic layers thick, as further verified by Figure 2a.

From atomically resolved STEM-HAADF images, two-dimensional (2-D) lattice strain mapping in the bulk of the nanoparticle core was performed, as demonstrated in Figure 2a,b (details on the method can be found in Supporting Information, Figures S3 and S4). It is very clear that these IMCS nanocatalysts exhibit a nonuniform strain distribution[23,26] on a 2D-projected plane rather than a uniform single strain value. This is because the Pt atoms are slightly relaxed at the surface compared to the bulk of the nanoparticle. We will demonstrate this later experimentally on comparing surface relaxation observed in noncycled and cycled nanocatalysts. On the basis of our calculations, we confirm that the lattice strain in the bulk of these Pt_3Fe_2 IMCS nanocatalysts relative to that in pure Pt/C is about −3%, which is in very good agreement with the theoretical value (−2.73%) for a 2D-projected plane viewed along the [110] zone axis (Supporting Information and Figure S3). The mass activity and catalytic activities of these nanocatalysts before and after electrochemical cycling 6000 times is represented in a bar plot in Figure 2c. Despite being highest among those of similar design reported in the literature,[18,24] the mass activity subsequently decreases on cycling following a sequential loss of electrochemical surface area (A_{Pt}).[19] We estimate that about 50 and 64% of the catalyst A_{Pt} is lost after 6000 and 10 000 cycles,

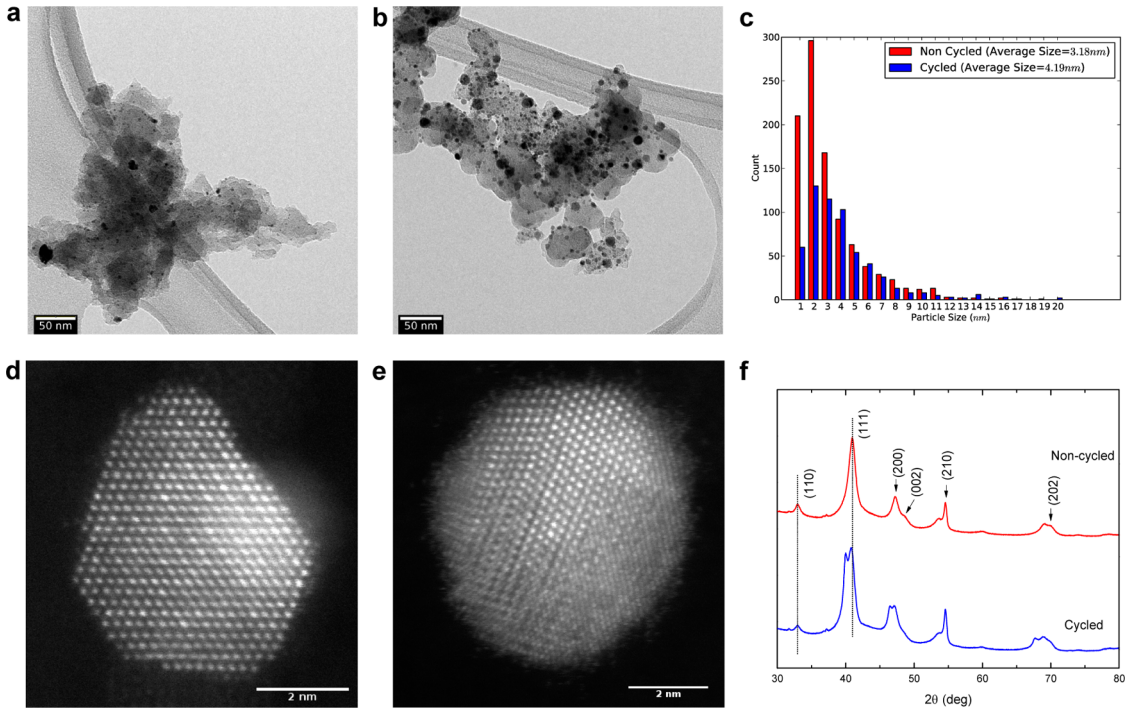

Figure 3. Particle size, morphology, and ordering. (a,b) TEM-BF images of as-prepared sample and the sample after 10 000 potential cycles, respectively, acquired at lower magnification. (c) Particle size distribution of a statistically systematic sample measured from BF acquisition of images with TEM. The average particle size of cycled nanocatalysts increased by about 1 nm compared to the noncycled one after treating over 10 000 potential cycles. (d,e) Atomic-resolution STEM-HAADF images of noncycled and cycled catalysts, respectively. (f) XRD data of the bulk sample.

respectively. However, it is quite intriguing to see a minimal decrease of 9% in the catalytic activity even after 6000 electrochemical cycles. While we attribute enhancement in catalytic activity primarily to lattice strain induced in the intermetallic Pt_3Fe_2 core, we demonstrate in the next section that these catalysts possess an enduring atomic order that is responsible for an extended longevity over 10 000 cycles.

Stability assessment on Pt_3Fe_2/C IMCSs was performed by employing three approaches: (1) electrochemical Pt surface area measurements over the course of 10 000 potential cycles,[19] (2) atomic-resolution STEM-HAADF characterization, and (3) X-ray diffraction on specimens to determine time evolution of its structural order, lattice contraction, and crystallite sizes. Electrochemical measurements that were carried out in a three-component cell (Methods) validated the Koutecky–Levich relationship,[27] ensuring a four-electron transfer following a complete reduction of O_2 to H_2O on the surface of IMCS nanocatalysts. A_{Pt} was calculated using a charge to surface area conversion of 210 μC cm^{-2}. These nanocatalysts were characterized over the course of 10 000 cycles using STEM-HAADF (Figure 3a–e) and XRD (Figure 3f) with two major themes: morphology and sustenance of chemical ordering in the intermetallic core.

Figure 3a,b shows bright-field (BF) images of noncycled and electrochemically cycled Pt_3Fe_2/C IMCSs, respectively, obtained under a conventional TEM at low magnifications. Though it is visually compelling to believe from the low-magnification BF images that these nanocatalysts show a significant increase in their sizes after cycling 10 000 times, such a conclusion is incorrect because the TEM observation is site-specific. Hence, we measured particle sizes of over 1030 nanocatalysts systematically sampled at various sites on the TEM grid to identify a statistical size distribution for both noncycled and cycled particles, as shown in Figure 3c. The average diameter of these nanoparticles experienced an increase of nearly 1 nm upon treating over 10 000 cycles, which is further validated by XRD analysis[19] that showed about 1.2 nm difference in the crystallite sizes. The expansion in the size distribution upon cycling indicates that there is a widely distributed particle size due to catalyst degradation. Such an increase in their sizes is due to enrichment in the nanocatalyst shell thickness, possibly by Ostwald ripening.[28] However, it is important to notice here that the increase is small compared to previous Pt–Fe catalyst designs,[18] owing to controlled degradation kinetics that will be demonstrated later in the section.

Changes in the surface morphology due to cycling are further examined, as shown in Figure 3d,e. Due to continuous Pt enrichment at the shell, the particles experienced a reduction in the number of high-index facets eventually leading to domains with low Miller indices and, hence, decreasing the total surface energy. However, the fact that this new surface formed

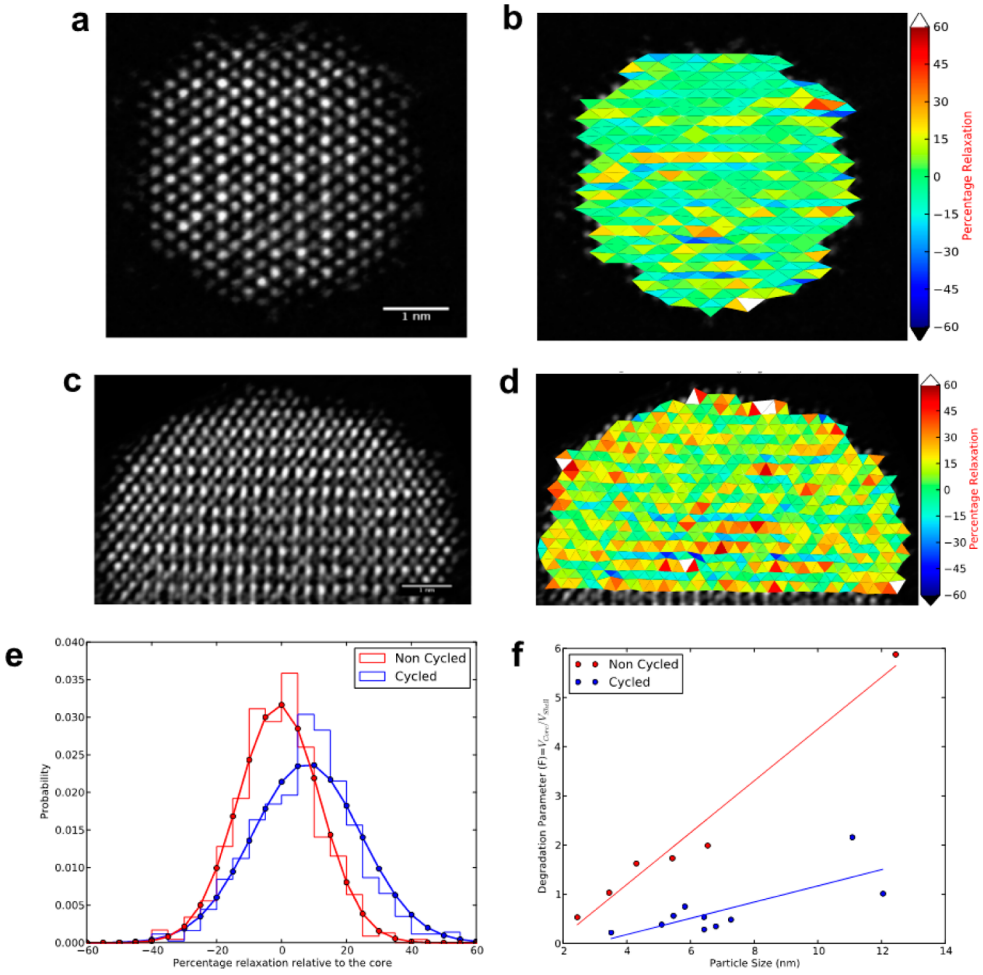

Figure 4. Surface relaxation and degradation. (a,c) STEM-HAADF images of noncycled and cycled (10 000) Pt_3Fe_2 IMCS nanocatalysts, respectively, viewed along the [110] zone axis. (b,d) Two-dimensional percentage relaxation mappings of the particles in (a) and (c), respectively. (e) Percentage relaxation distribution plotted from the data obtained at each color segment shown in (b) and (d). The plot demonstrates that the cycled particles exhibit relatively more surface relaxation compared to noncycled ones, similar to the one discussed in (a) and (b). (f) Degradation parameter is plotted across various particle sizes for both noncycled and cycled nanocatalysts. Region between two regimes is the zone of degradation. Based on static core−dynamic shell constraint, the degradation parameter exhibits an inverse proportionality with the volume of the shell.

through cycling is composed of atoms with bond lengths that are more relaxed relative to the bulk should not be overlooked. It is important to notice here that, despite a constant enrichment of the Pt shell over 10 000 electrochemical cycles, the particle still retained its core ordering as revealed by the XRD pattern in Figure 3f. Locating two small shoulders at 2θ values of 49.2° (due to (002) reflection) and 70.6° (due to (202) reflection) corresponds to lattice compression from cubic to a tetragonal ordered Pt−Fe type alloy structure. A rightward shift in the (111) peak toward more negative 2θ values indicates Pt enrichment upon sequential cycling. Most importantly, the presence of the (110) superlattice reflection at around $2\theta = 39.77°$ confirms sustained atomic ordering even after 10 000 potential cycles. This result is consistent with our atomic-scale STEM analysis, as shown in Figure 4a,c, and we attribute an enhanced durability among these nanocatalysts compared to other Pt−Fe systems to such endurance in chemical order despite cycling.

STEM-HAADF characterization of systematically sampled nanoparticles and the XRD measurements on the bulk sample confirm that degradation mechanisms are operative during cycling, and yet, the local chemical order at the core is retained. This is possible only if the ordered core remains unaffected on subsequent cycling because the phase transformation toward forming new ordered cores is thermodynamically not favorable. This static core regime will consequently imply that the increase in particle sizes (Figure 3c) is due to a Pt shell enrichment with the core virtually intact. To our knowledge, this static core−dynamic shell (SCDS) regime is being reported for the first time. In order to explain the existence of the SCDS regime in these Pt_3Fe_2 IMCS nanocatalysts, we atomically resolved both noncycled and cycled particles in STEM-HAADF mode to perform a 2-D surface

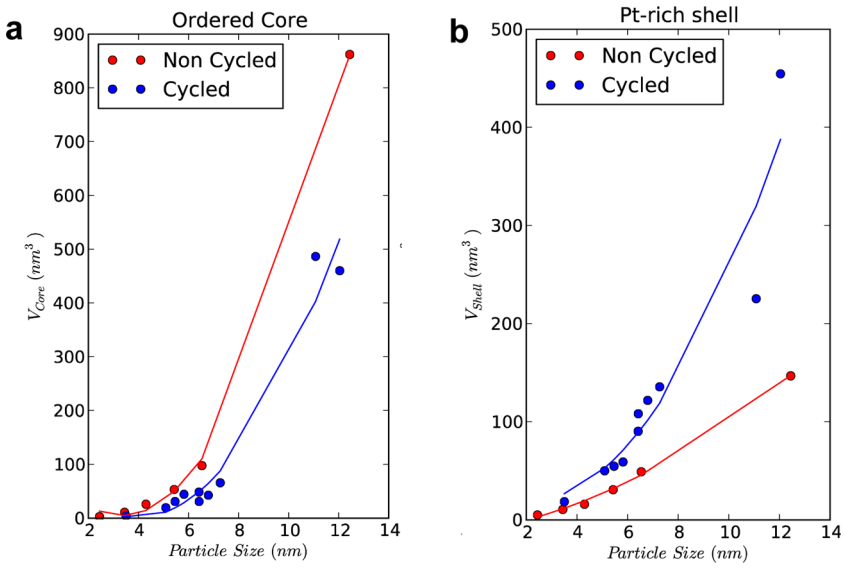

Figure 5. Ordered core and disordered shell volumes. (a) Plot of ordered core volume *versus* particle size. Particles in the size range between 3.2 and 4.2 nm are found to retain comparable core volumes despite 10 000 potential cycles. (b) Plot of disordered shell *versus* particle size. It is evident that, upon cycling, particles in the size range of 3.2 to 4.2 nm, despite possessing comparable core volumes, however, showed an increase in their shell volumes due to Pt shell enrichment.

relaxation mapping with respect to the core, as shown in Figure 4a–e. We found a significant atomic relaxation in the Pt-rich shells of cycled nanocatalysts as quantified in the colormap shown. We believe that this is due to redeposition of Pt atoms on the shells, made possible by Ostwald ripening. ORR and catalyst layer degradation operate continuously throughout the lifetime of a fuel cell, and the deposition of Pt atoms on the oxidized catalyst surface might have led to the observed relaxation. We infer through a rigorous statistical treatment shown in Figure 4e that the cycled nanocatalyst showed a surface relaxation of about 30% (relative to the core) upon 10 000 potential cycles.

A newly developed peak at 39.9° in the XRD pattern (Figure 3f) is attributed to Pt, which is further supported by Pt/Fe compositional analyses plotted in Supporting Information Figure S5, which was obtained by the SEM-EDXS analysis technique (10 measurements per sample) at an accelerating voltage of 20 kV with a 15 mm working distance. The evolution of this compositional measurement clearly highlights that the degradation kinetics is slow with an energy-driven ripening. A steep increase in the Pt/Fe ratios during the initial 3000 cycles is possibly because of higher probability of encountering smaller particles leading to a thermodynamically driven aggregation to form larger particles. The compositional evolution after 3000 cycles reiterates the size dependency of degradation kinetics possibly due to Ostwald ripening[29] at the nanoscale. In that case, it is quite reasonable to predict that a critical size is approached after successive cycling beyond which Ostwald ripening would cease to operate. Unlike disordered core–shell and bimetallic catalysts that are expected to exhibit significant decrease in activity, the IMCS nanocatalysts are more likely to continue functioning at relatively higher activities beyond critical ripening size owing to their SCDS regime.

Evolution of structural ordering with cycling is quantified in terms of a "degradation parameter (DP)" as demonstrated in Figure 4f. Here we define the DP of a nanocatalyst as the volume ratio of its ordered core to disordered shell with a fairly reasonable assumption that a nanoparticle is spherical. The shell and core volumes are calculated by measuring their respective spherical diameters from STEM-HAADF images (Supporting Information, Figure S6 and Table S1). A statistically systematic sample is chosen, and the DP calculated at different particle sizes is plotted. The zone of degradation that exists between noncycled and cycled regimes is unique to different IMCS designs, and its calculated area will hence provide an insight into the activity loss due to catalyst degradation. Based on SCDS constraint, the DP bears witness to an inverse proportionality with respect to disordered shell volume. Conversely, it is therefore possible to predict from our measurements the enrichment due to Pt redeposition in any nanocatalyst particle within the zone of degradation. The degradation parameter calculated for any IMCS nanocatalyst will serve as its design index indicative of structure evolution, stability, and durability during the lifetime of a fuel cell. The evolution of the volumes of cores and shells is plotted as a function of particle size in Figure 5a,b that further confirms the SCDS regime. Catalysts lying in the range corresponding to their average diameters for noncycled and cycled conditions (3.2 to 4.2 nm) clearly exhibit ordered cores with almost no change in their volumes despite treating over 10 000 potential cycles,

as shown in Figure 5a. Interestingly, their corresponding shell volumes showed an increase upon cycling, as demonstrated in Figure 5b and Table S1.

CONCLUSIONS

In summary, our current work introduces an ordered Pt_3Fe_2 core encapsulated in a bilayer Pt-rich shell as the newest intermetallic core–shell nanocatalyst member of the Pt–Fe system for the ORR. Enhancement in the catalytic activity and durability over existing Pt–Fe nanocatalyst designs is attributed to strained lattice and sustained atomic order, respectively. The degradation kinetics is slow due to their static core–dynamic shell regimes during electrochemical cycling. Evolution of structural ordering over the lifetime of these nanocatalysts is quantified into a design index that serves as a direct measure of catalyst degradation and, hence, redefining a new design methodology for next generation fuel cell nanocatalysts.

METHODS

Sample Preparation. The Pt_3Fe_2/C IMCS nanocatalysts were prepared *via* a wet impregnation technique[19] with Pt/C nanoparticles as precursors supported on Vulcan XC-724R carbon. Pt/C were prepared as a first step by employing the polyol method reported previously.[30] First, 500 mg of 20 wt % precursors was ultrasonicated for about 1.5 h in order to disperse them uniformly in 120 mL of water. Then, 0.1381 g of $Fe(NO_3)_3 \cdot 9H_2O$ salt (Alfa Aesar, 99.99% Fe basis) and 1 mL of 1 M HNO_3 were added to the suspension. Water was evaporated by continuous stirring for 0.5 h. The dried samples remaining were then ground using a glass mortar and then annealed at 800 °C for 3 h in a Lindberg Blue tube furnace. Samples were heated at a rate of 10 °C min^{-1}, annealed, and then cooled in a 92% Ar/8% H_2 reducing atmosphere.

Electrochemical Measurements were carried out in a three-component cell[19] comprising a large surface area Pt and Au gauzes as counter electrodes and Hg/Hg_2SO_4 (1 M Na_2SO_4) reference electrodes (MSE), with 0.1 M perchloric acid ($HClO_4$) solution as electrolyte. Further, the reference electrode was calibrated using the H_2 oxidation/reduction reaction on a large surface area Pt electrode. The potentials reported here were all referenced *versus* the reversible H_2 electrode (RHE). Initially, the working electrodes were cycled at 50 mV s^{-1} between 0.06 and 1.3 V for 70 cycles to condition the electrodes. ORR measurements were carried out between 0 and 1.2 V *versus* the RHE in oxygen-saturated 0.1 M $HClO_4$ solutions. A sweep rate of 10 mV s^{-1} was employed with the rotating ring disk electrode (RDE) operating at 1600 rpm. Measurements were also made at other rpm values to validate the Koutecky–Levich relationship. Electrochemical assessment was performed at room temperature and using high-purity (18 MΩ) water. A_{Pt} was calculated using a charge to surface area conversion factor of 210 μC cm^{-2}.

Scanning Transmission Electron Microscopy (STEM) characterization of various catalyst nanoparticles was carried out at the Canadian Centre for Electron Microscopy. The low-magnification bright-field micrographs (Figure 3a,b) were acquired in a Philips CM12 TEM operated at 120 kV. High-resolution bright-field TEM imaging (Figure 1a) was performed in a FEI Titan microscope equipped with an hexapole spherical aberration corrector of the image forming lens and operated at 300 kV. Atomically resolved high-angle annular dark-field (HAADF) images were acquired in a FEI Titan cubed TEM, equipped with two hexapole spherical aberration correctors of the probe and image forming lenses. It was operated in STEM mode at an accelerating voltage of 300 kV.

STEM-HAADF images are generated by collecting electrons scattered at high angles on passing through the samples, using a Fischione HAADF detector, and the acquired image intensity is roughly proportional to $Z^{1.6}$, where Z is the atomic number of scattering atoms.

X-ray Diffraction. XRD patterns for noncycled and cycled specimens were obtained using a Bruker D8 Advance diffractometer with Bragg–Brentano geometry employing a Cu Kα source. The collection angle extended from 20 to 90° with a step size of 0.02° and an acquisition time of 3 s per step.

Conflict of Interest: The authors declare no competing financial interest.

Acknowledgment. S.P., M.B., and G.A.B. are grateful to NSERC for Discovery, APC (CaRPE-FC) and Strategic grants supporting this work. The microscopy was carried out at the Canadian Centre for Electron Microscopy (CCEM), a national facility supported by the NSERC and McMaster University. C.B. acknowledges the financial support from NRC. C.B. also thanks Tom Zahran and Liang Chen (NRC, Ottawa) for their assistance in sample preparation.

Supporting Information Available: Supplementary figures. This material is available free of charge *via* the Internet at http://pubs.acs.org.

REFERENCES AND NOTES

1. Lu, Y.; Gasteiger, H.; Crumlin, E.; McGuire, R.; Shao-Horn, Y. Electrocatalytic Activity Studies of Select Metal Surfaces and Implications in Li-Air Batteries. *J. Electrochem. Soc.* **2010**, *157*, A1016–A1025.
2. Zhong, C. J.; Luo, J.; Fang, B.; Wanjala, B. N.; Njoki, P. N.; Loukrakpam, R.; Yin, J. Nanostructured Catalysts in Fuel Cells. *J. Nanotechnol.* **2010**, *21*, 062001.
3. Debe, M. K. Electrocatalyst Approaches and Challenges for Automotive Fuel Cells. *Nature* **2012**, *486*, 43–51.
4. Gasteiger, H. A.; Kocha, S. S.; Sompalli, B.; Wagner, F. T. Activity Benchmarks and Requirements for Pt, Pt-Alloy, and Non-Pt Oxygen Reduction Catalysts for PEMFCs. *Appl. Catal., B* **2005**, *56*, 9–35.
5. Mukerjee, S.; Srinivasan, S.; Soriaga, M. P.; McBreen, J. Effect of Preparation Conditions of Pt Alloys on Their Electronic, Structural, and Electrocatalytic Activities for Oxygen Reduction—XRD, XAS, and Electrochemical Studies. *J. Phys. Chem.* **1995**, *99*, 4577–4589.
6. Toda, T.; Igarashi, H.; Uchida, H.; Watanabe, M. Enhancement of the Electroreduction of Oxygen on Pt Alloys with Fe, Ni, and Co. *J. Electrochem. Soc.* **1999**, *146*, 3750–3756.
7. Xiong, L.; Manthiram, A. Effect of Atomic Ordering on the Catalytic Activity of Carbon Supported PtM (M = Fe, Co, Ni, and Cu) Alloys for Oxygen Reduction in PEMFCs. *J. Electrochem. Soc.* **2005**, *152*, A697–A703.
8. Alloyeau, D.; Ricolleau, C.; Mottet, C.; Oikawa, T.; Langlois, C.; Bouar, Y.; Le Braidy, N.; Loiseau, A. Size and Shape Effects on the Order–Disorder Phase Transition in CoPt Nanoparticles. *Nat. Mater.* **2009**, *8*, 940–946.
9. Stephens, I. E. L.; Bondarenko, A. S.; Perez-Alonso, F. J.; Calle-Vallejo, F.; Bech, L.; Johansson, T. P.; Jepsen, A. K.; Frydendal, R.; Knudsen, B. P.; Rossmeisl, J.; *et al.* Tuning the Activity of Pt(111) for Oxygen Electroreduction by Subsurface Alloying. *J. Am. Chem. Soc.* **2011**, *133*, 5485–5491.
10. Greeley, J.; Stephens, I. E. L.; Bondarenko, A. S.; Johansson, T. P.; Hansen, H. A.; Jaramillo, T. F.; Rossmeisl, J.; Chorkendorff, I.; Nørskov, J. K. Alloys of Platinum and Early Transition Metals as Oxygen Reduction Electrocatalysts. *Nat. Chem.* **2009**, *1*, 552–556.
11. Stamenkovic, V. R.; Mun, B. S.; Arenz, M.; Mayrhofer, K. J. J.; Lucas, C. A; Wang, G.; Ross, P. N.; Markovic, N. M. Trends in Electrocatalysis on Extended and Nanoscale Pt-Bimetallic Alloy Surfaces. *Nat. Mater.* **2007**, *6*, 241–247.
12. Luo, J.; Kariuki, N.; Han, L.; Wang, L.; Zhong, C. J.; He, T. Preparation and Characterization of Carbon-Supported

PtVFe Electrocatalysts. *Electrochim. Acta* **2006**, *51*, 4821–4827.
13. Wang, J. X.; Inada, H.; Wu, L.; Zhu, Y.; Choi, Y.; Liu, P.; Zhou, W. P.; Adzic, R. R. Oxygen Reduction on Well-Defined Core−Shell Nanocatalysts: Particle Size, Facet, and Pt Shell Thickness Effects. *J. Am. Chem. Soc.* **2009**, *131*, 17298–17302.
14. Sun, S. Monodisperse FePt Nanoparticles and Ferromagnetic FePt Nanocrystal Superlattices. *Science* **2000**, *287*, 1989–1992.
15. Stamenkovic, V. R.; Fowler, B.; Mun, B. S.; Wang, G.; Ross, P. N.; Lucas, C. A; Marković, N. M. Improved Oxygen Reduction Activity on Pt3Ni(111) *via* Increased Surface Site Availability. *Science* **2007**, *315*, 493–497.
16. Wang, D.; Xin, H. L.; Hovden, R.; Wang, H.; Yu, Y.; Muller, D. A.; Disalvo, F. J.; Abruña, H. D. Structurally Ordered Intermetallic Platinum−Cobalt Core−Shell Nanoparticles with Enhanced Activity and Stability as Oxygen Reduction Electrocatalysts. *Nat. Mater.* **2012**, *11*, 1–7.
17. Ouyang, G.; Zhu, W. G.; Sun, C. Q.; Zhu, Z. M.; Liao, S. Z. Atomistic Origin of Lattice Strain on Stiffness of Nanoparticles. *Phys. Chem. Chem. Phys.* **2010**, *12*, 1543–1549.
18. Li, X.; An, L.; Wang, X.; Li, F.; Zou, R.; Xia, D. Supported Sub-5nm Pt−Fe Intermetallic Compounds for Electrocatalytic Application. *J. Mater. Chem.* **2012**, *22*, 6047–6052.
19. Chen, L.; Chan, M. C. Y.; Nan, F.; Bock, C.; Botton, G. A.; Mercier, P. H. J.; MacDougall, B. R. Compositional and Morphological Changes of Ordered PtxFey/C Oxygen Electroreduction Catalysts. *ChemCatChem* **2013**, *5*, 1449–1460.
20. Chen, L.; Bock, C.; Mercier, P.; MacDougall, B. Ordered Alloy Formation for Pt_3Fe/C, PtFe/C and $Pt_{5.75}Fe_{5.75}Cuy/CO_2$-Reduction Electro-catalysts. *Electrochim. Acta* **2012**, *77*, 212–224.
21. Vasiliev, M. Surface Effects of Ordering in Binary Alloys. *J. Phys. D: Appl. Phys.* **1999**, *30*, 3037–3070.
22. Yu, T. H.; Sha, Y.; Merinov, B. V.; Goddard, W. A. Improved Non-Pt Alloys for the Oxygen Reduction Reaction at Fuel Cell Cathodes Predicted from Quantum Mechanics. *J. Phys. Chem. C* **2010**, *114*, 11527–11533.
23. Gan, L.; Yu, R.; Luo, J.; Cheng, Z.; Zhu, J. Lattice Strain Distributions in Individual Dealloyed Pt−Fe Catalyst Nanoparticles. *J. Phys. Chem. Lett.* **2012**, *3*, 934–938.
24. Chan, M. C. Y.; Chen, L.; Nan, F.; Britten, J. F.; Bock, C.; Botton, G. A. Structure, Ordering, and Surfaces of Pt−Fe Alloy Catalytic Nanoparticles from Quantitative Electron Microscopy and X-ray Diffraction. *Nanoscale* **2012**, *4*, 7273–7279.
25. Chen, H.; Yu, Y.; Xin, H. L.; Newton, K. A.; Holtz, M. E.; Wang, D.; Muller, D. A.; Abruña, H. D.; DiSalvo, F. J. Coalescence in the Thermal Annealing of Nanoparticles: An *In Situ* STEM Study of the Growth Mechanisms of Ordered Pt−Fe Nanoparticles in a KCl Matrix. *Chem. Mater.* **2013**, *25*, 1436–1442.
26. Johnson, C. L.; Snoeck, E.; Ezcurdia, M.; Rodríguez-González, B.; Pastoriza-Santos, I.; Liz-Marzán, L. M.; Hytch, M. J. Effects of Elastic Anisotropy on Strain Distributions in Decahedral Gold Nanoparticles. *Nat. Mater.* **2008**, *7*, 120–124.
27. Bard, A. J.; Faulkner, L. R. *Electrochemical Methods: Fundamentals and Applications*; Wiley: New York, 2001; Vol. 677, p 833.
28. Shao-Horn, Y.; Sheng, W. C.; Chen, S.; Ferreira, P. J.; Holby, E. F.; Morgan, D. Instability of Supported Platinum Nanoparticles in Low-Temperature Fuel Cells. *Top. Catal.* **2007**, *46*, 285–305.
29. Alloyeau, D.; Prévot, G.; Le Bouar, Y.; Oikawa, T.; Langlois, C.; Loiseau, A.; Ricolleau, C. Ostwald Ripening in Nanoalloys: When Thermodynamics Drives a Size-Dependent Particle Composition. *Phys. Rev. Lett.* **2010**, *105*, 1–4.
30. Bock, C.; Paquet, C.; Couillard, M.; Botton, G. A.; MacDougall, B. R. Size-Selected Synthesis of PtRu Nano-Catalysts: Reaction and Size Control Mechanism. *J. Am. Chem. Soc.* **2004**, *126*, 8028–8037.